PALEOENVIRONMENT

A global environmental crisis 42,000 years ago

Alan Cooper[1,2]*†, Chris S. M. Turney[3]*†, Jonathan Palmer[3], Alan Hogg[4], Matt McGlone[5], Janet Wilmshurst[5,6], Andrew M. Lorrey[7], Timothy J. Heaton[8], James M. Russell[9], Ken McCracken[10], Julien G. Anet[11], Eugene Rozanov[12,13,14], Marina Friedel[12], Ivo Suter[15], Thomas Peter[12], Raimund Muscheler[16], Florian Adolphi[17], Anthony Dosseto[18], J. Tyler Faith[19], Pavla Fenwick[20], Christopher J. Fogwill[21], Konrad Hughen[22], Mathew Lipson[23], Jiabo Liu[24], Norbert Nowaczyk[25], Eleanor Rainsley[21], Christopher Bronk Ramsey[26], Paolo Sebastianelli[27], Yassine Souilmi[28], Janelle Stevenson[29,30], Zoë Thomas[3], Raymond Tobler[28], Roland Zech[31]

Geological archives record multiple reversals of Earth's magnetic poles, but the global impacts of these events, if any, remain unclear. Uncertain radiocarbon calibration has limited investigation of the potential effects of the last major magnetic inversion, known as the Laschamps Excursion [41 to 42 thousand years ago (ka)]. We use ancient New Zealand kauri trees (*Agathis australis*) to develop a detailed record of atmospheric radiocarbon levels across the Laschamps Excursion. We precisely characterize the geomagnetic reversal and perform global chemistry-climate modeling and detailed radiocarbon dating of paleoenvironmental records to investigate impacts. We find that geomagnetic field minima ~42 ka, in combination with Grand Solar Minima, caused substantial changes in atmospheric ozone concentration and circulation, driving synchronous global climate shifts that caused major environmental changes, extinction events, and transformations in the archaeological record.

O ver the recent past, Earth's magnetic field has steadily weakened (~9% in the past 170 years), and this, along with the current rapid movement of the magnetic North Pole, has increased speculation that a field reversal may be imminent (*1, 2*). The estimated economic impacts of such a reversal have focused on the increased exposure to extreme solar storms, with multibillion-dollar daily loss estimates (*3*) likely to be conservative. One of the best opportunities to study the impacts of extreme changes in Earth's magnetic field is the Laschamps Excursion (hereafter Laschamps)— a recent, relatively short-duration (<1000 year) reversal ~41 thousand years ago (ka) (*4*). Sedimentary and volcanic deposits indicate a weakening of the magnetic field intensity to <28% of current levels during the reversed phase of the Laschamps and, notably, as little as 0 to 6% during the preceding transition as polarity switched (Fig. 1 and supplementary materials) (*1, 2, 5*).

Studies of Greenland ice cores have failed to reveal marked impacts in high-latitude paleoclimate associated with Laschamps (*5, 6*), and this observation has underpinned the current view that there is no relationship between geomagnetic reversals and climate or environmental changes. However, the markedly increased levels of solar and cosmic radiation reaching Earth's atmosphere because of the weakened geomagnetic field are likely to have increased atmospheric ionization and decreased stratospheric ozone levels, potentially generating regional climatic impacts, particularly in lower latitudes (*7–9*). In this regard, it is notable that many environmental records around the Pacific Basin appear to detail a major (and often sustained) change in behavior ~40 to 42 ka, including local glacial maxima in Australasia and the Andes (*7, 10*), long-term shifts in atmospheric circulation patterns (*11, 12*), and continent-wide aridification and megafaunal extinction in Australia (*4, 13–16*). The same period in North America saw the rapid, pronounced expansion of the Laurentide Ice Sheet (LIS) from a local minimum close to 42 ka (*17–19*). Many of these records document a long-term phase shift into a glacial state that persisted until the transition into the Holocene (~11.6 ka), in direct contrast to the Atlantic Basin records of millennial-scale abrupt and extreme changes associated with stadial-interstadial events.

Although the Pacific Basin environmental changes appear broadly coincident with the Laschamps, the lack of knowledge about the exact timing and duration of the geomagnetic excursion has greatly limited the ability to examine whether it played any role. In addition, chronological uncertainties are complicated in radiocarbon-dated terrestrial and marine records around the Laschamps because of the elevated production of ^{14}C and ^{10}Be, cosmogenic radionuclides resulting from the substantial increase in high-energy cosmic radiation reaching the upper atmosphere. The high ^{10}Be flux has been well described from Greenland and Antarctic ice core records (*6, 20, 21*), which reveal synchronous century-long ^{10}Be peaks across the Laschamps that appear to reflect a series of pronounced Grand Solar Minima (GSM; prolonged periods of low solar activity similar to the Spörer and Maunder Minima: 1410 to 1540 CE and 1645 to 1715 CE), with unknown climate impacts (*20, 21*). By contrast, the associated atmospheric ^{14}C changes remain poorly constrained (*22*), preventing precise calibration (*23*).

Radiocarbon changes across the Laschamps

In this study, we performed detailed radiocarbon analyses of ancient kauri (*Agathis australis*) trees preserved in northern New Zealand wetlands (*24*) to generate a contiguous reconstruction of atmospheric ^{14}C across the Laschamps (see supplementary materials). We compared a series of radiocarbon measurements across multiple kauri trunk cross sections to identify variations in atmospheric radiocarbon at a highly resolved level. A 1700-year record from a tree recovered from Ngāwhā, Northland, is

particularly important because it spans the period of greatest change in ^{14}C, including an apparent weakening of the magnetic field before the Laschamps. The growth of the Ngāwhā tree is relatively suppressed compared with both modern kauri and other late Pleistocene kauri, and there is a marked

decrease in tree-ring width that coincides with the weakest phase of the geomagnetic field (supplementary materials). We spliced the kauri tree ^{14}C series into the radiocarbon dataset reported from the [230]Th-dated Hulu Cave speleothem (22) to provide an absolute (calendar) time scale (Fig. 1). Our 40-year–

resolved reconstruction (Fig. 1) shows major changes in atmospheric radiocarbon before and during the Laschamps (23), closely matching reconstructions of the virtual geomagnetic pole [positions and geomagnetic intensity (1, 5)]. A comparison of the kauri-Hulu ^{14}C with the paleomagnetic intensity data indicates that

Fig. 1. Atmospheric radiocarbon changes across the Laschamps geomagnetic excursion and compared with key environmental datasets. (**A** and **B**) Kauri ^{14}C ages and Δ^{14}C values before and through the Laschamps (colored symbols) compared with Hulu Cave radiocarbon values (open symbols) (22). The arrow denotes the peak in Δ^{14}C coincident with a prominent GSM (see below). A short ^{14}C plateau 42.20 to 42.04 ka occurs around halfway through the steep rise in ^{14}C, which is consistent with Cariaco Basin (40) and demonstrates that this is a robust feature in the record. B.P., before present (1950 CE); Mag., magnetic. Error bars indicate 1σ. (**C**) Relative paleomagnetic intensity curve aligned to the Greenland ice core record reported from Black Sea sediments (5). (**D**) Normalized Greenland [10]Be flux (light blue line) (20) compared with modeled ^{14}C production rates from the kauri-Hulu dataset (thick black line). The amplified peaks in [10]Be during the weakened paleomagnetic field are consistent with increased ionizing radiation during GSM (arrows; see supplementary materials). (**E**) North Greenland Ice Core Project (NGRIP) δ^{18}O record reported on the GICC05 (+265 years) time scale B.P.; Greenland interstadial (warming) events 11 to 9 are shown (41), along with the weak Greenland stadial (GS-10), which may represent a local Greenland signal of abrupt cooling interrupting a larger interstadial event originally consisting of GI-10 and GI-9 (29, 30). (**F**) Sediment total reflectance (refl-L*) measurements from Cariaco Basin (250-point running mean) showing the absence of a clear GS-10 signal (30). The reversed geomagnetic polarity (light-gray column) and flanking transition phases (dark gray) are indicated, with the latter being the weakest periods of Earth's magnetic field and closely coincident with GS-11 and GS-10.
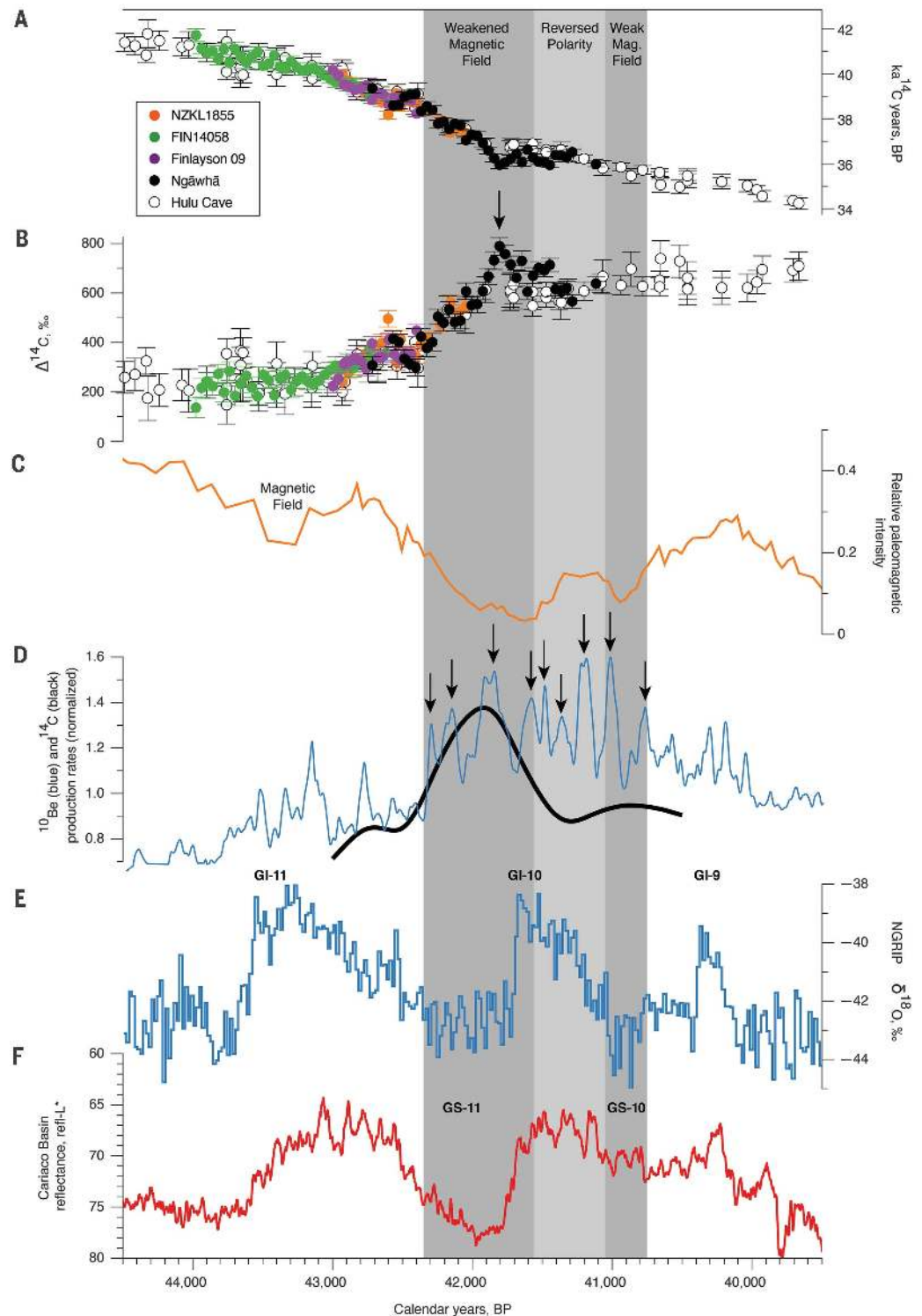
the reversed phase of the geomagnetic field (and associated partial recovery) defining the Laschamps sensu stricto occurred at 41.56 to 41.05 ka (supplementary materials).

By modeling ^{14}C-production rates from our kauri Δ^{14}C record, it is possible to precisely align to the ice core time scale by using [10]Be records (21). Across this period, we infer that the Greenland ice core 2005 (GICC05) time scale is 265 years younger than the Hulu Cave time scale (95.4% range: 160 to 310 years) (Fig. 1 and fig. S15), which is considerably more precise than previous comparisons (21). Notably, the steep rise in Δ^{14}C commences at 42.35 ka, with a peak value of 782 per mil (‰) occurring at 41.8 ka, 300 years before the full Laschamps reversal. This is the highest atmospheric ^{14}C concentration yet reported of the pre-anthropogenic radiocarbon time scale (22, 23, 25) (see supplementary materials). The peak Δ^{14}C value reported here occurs during the most weakened phase of the geomagnetic field (5) and is associated with a prominent GSM recorded by [10]Be flux

(20) (Fig. 1 and supplementary materials), when the weakened solar interplanetary magnetic field allowed enhanced input of galactic cosmic rays (GCRs) into the upper atmosphere. This kauri-Hulu record provides a precise radiocarbon calibration curve for this period, permitting a detailed recalibration of wider environmental changes to test synchrony between events while also enabling us to investigate the potential climate drivers during the Laschamps.

Global chemistry-climate modeling

To explore the impacts of a greatly weakened geomagnetic field on atmospheric ionization, chemistry, and dynamics, we undertook a series of simulations using a global chemistry-climate model, SOCOL-MPIOM (8) (see supplementary materials). First, the global conditions before the Laschamps were modeled by using modern values of the geomagnetic dipole moment (M) and average solar modulation potential (ϕ) of 800 MV (equivalent to the modern value). After a

398-year spin-up, three 72-year–long simulations (from which the last 60 years were used for analysis) were branched off to study the Laschamps and two additional solar states likely to influence atmospheric ionization: a reference run keeping M = 100% current and ϕ = 800 MV (experiment REF); the Laschamps with weakened geomagnetic field (M = 0% current, ϕ = 800 MV; experiment M0P800) (2); and a Laschamps weakened geomagnetic field plus GSM when the decreased geomagnetic field and the reduced solar modulation potential greatly increase the GCR ionization rate in Earth's atmosphere (M = 0% current, ϕ = 0 MV; experiment M0P0).

Although our simulation for the weakened magnetic field during the Laschamps (M0P800) showed modest but significant changes in atmospheric chemistry and climate (see supplementary materials), the scenario for Laschamps plus GSM (M0P0) showed greatly amplified impacts, most notably during the boreal winter and austral summer (December to February) (Figs. 2 and 3 and figs. S18 to S30).

Fig. 2. The impact of a weakened geomagnetic field and GSM on global chemistry. (**A** to **C**) Simulated anomalies in boreal winter and austral summer (relative to experiment REF; December to February) atmospheric chemistry [HOx, NOx, and O$_3$ in (A), (B), and (C), respectively] for a weakened magnetic field during the Laschamps plus GSM (M = 0, ϕ = 0); colored areas denote 10% significance. (**D**) Total ozone column change [Dobson units (DU)]; hatched areas denote 10% significance level.
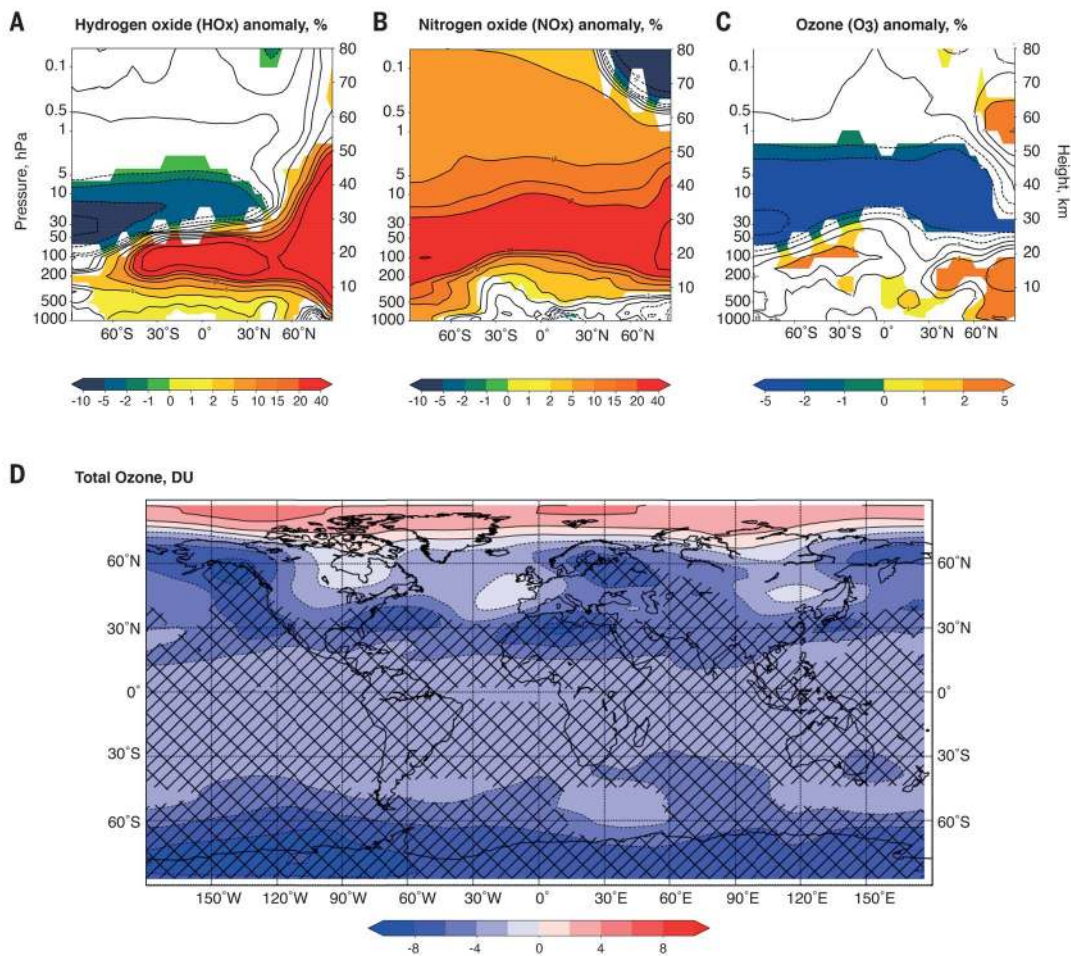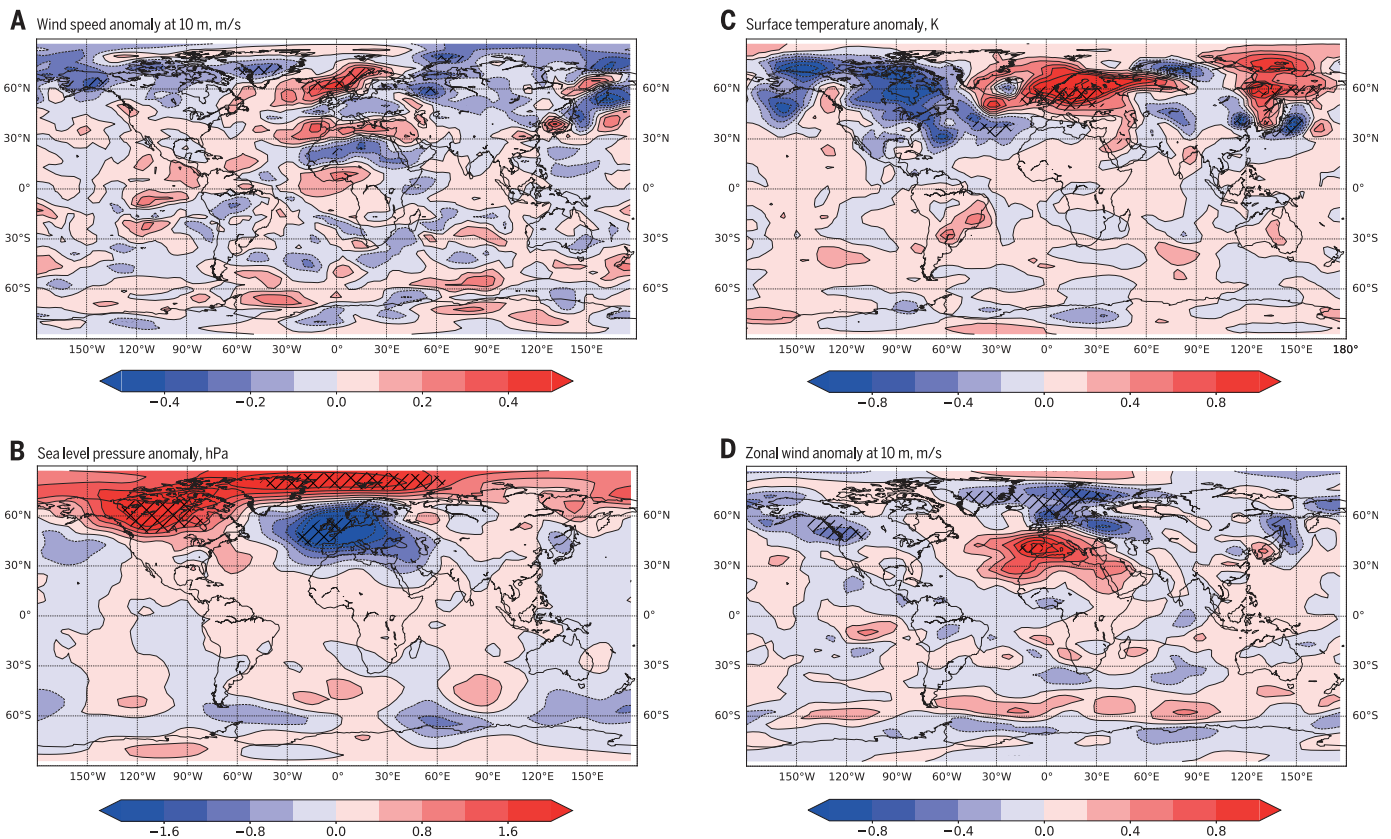
Fig. 3. The impact of a weakened geomagnetic field and GSM on global climate. (**A** to **D**) Simulated anomalies in boreal winter and austral summer (relative to experiment REF; December to February) wind speed at 10 m, sea-level pressure, surface temperature, and zonal wind [(A) to (D), respectively] for a weakened magnetic field during the Laschamps plus GSM (M = 0, φ = 0); hatched areas denote 10% significance level.

Our results yield a large increase in atmospheric ionization from GCRs, resulting in an enhanced production of hydrogen and nitrogen oxides (HOx and NOx, respectively) (Fig. 2, A and B) (8) down to very low altitudes. The increased HOx and NOx concentrations influenced ozone levels over the entire atmosphere, decreasing the O_3 mixing ratio in the stratosphere (~5%) while increasing the O_3 mixing ratio in the troposphere, with the greatest changes observed over Antarctica (~5%) (Fig. 2, C and D).

We find that decreasing stratospheric O_3 concentrations had climatic impacts over the mid- to high latitudes in both hemispheres (Fig. 3). In the Northern Hemisphere, this changed the equator-to-pole temperature gradient, weakening the Arctic polar vortex and leading to a net warming effect in the lower polar stratosphere. We postulate that this positive temperature anomaly was further amplified by an increase in the Brewer-Dobson Circulation, which would have, among other effects, led to adiabatic warming of air masses sinking from upper to lower stratospheric heights. The reason for the increased Brewer-Dobson Circulation may originate from

a wavier jet stream, reaching higher velocities at the Northern Hemisphere latitudes with the most pronounced orographic barriers and increasing gravity-wave production, which subsequently propagated vertically up through the atmospheric column (26). The lower atmosphere responded to those factors with sea-level pressure increases over the Arctic and North America and decreases over Western Europe, with parallel changes in surface temperature. These changes resemble a negative phase of the Arctic Oscillation (AO) and North Atlantic Oscillation (NAO), consistent with reanalysis studies (27). In the Southern Hemisphere, decreasing stratospheric O_3 appears to be associated with small changes in the mid-latitude airflow (Fig. 3) and subtropical precipitation patterns (see supplementary material) (8). Because the significance is <10%, an ensemble of longer model runs is required to confirm this finding.

Although previous studies have suggested that snowfall over Greenland is summer dominated during glacial conditions (28), the model predictions of pronounced boreal winter Arctic surface cooling are potentially important in the context of the Greenland ice

core records spanning this period. It is notable that the two weakest phases of geomagnetic field strength during the Laschamps closely coincide with the cold Greenland stadials 11 (GS-11) and GS-10 (Fig. 1). Furthermore, GS-10 and the following brief interstadial GI-9 have a number of atypical features that have led to suggestions that they might represent the interruption of a single long warm interstadial (composed of GI-10 and GI-9, as seen in other records such as Cariaco Basin) (Fig. 1) by an abrupt cold phase, likely related to an expansion in North Atlantic sea-ice extent, which changed the climatic gradient between the mid-latitudes and Greenland (29, 30) (supplementary materials). As a result, the climatic impacts of the Laschamps may have been obscured by the way they are represented in the Greenland ice core records.

Pacific climate and environmental impacts

In the Northern Hemisphere, it remains difficult to disentangle the similarly timed impacts of Laschamps from Greenland stadial-interstadial events, early glacial advances, and the expansion of anatomically modern humans (AMHs) (4, 31). Therefore, to isolate the potential impacts of

Fig. 4. Climatic and environmental changes across the 42 ka Adams Event. (**A**) NGRIP δ18O (*41*). HE4 refers to Heinrich Event 4 within GS-9. (**B** and **C**) Neanderthal extinction in Europe (40.9 to 40.5 ka) recalibrated with the kauri-Hulu calibration curve (B) and arrival of AMHs in Europe (C) and development of Initial Upper Paleolithic cultures (*37*). (**D**) Early cave art and cave utilization across both Europe and Southeast Asia (*34–36*). (**E**) Rapid expansion of LIS after a minimum extent at 42 ka calendar B.P. that commenced immediately before or during the Laschamps (*17–19*). (**F**) Kauri and Hulu Cave Δ14C values; colored solid circles denote individual trees (key in Fig. 1). Error bars indicate 1σ. (**G**) Migration south of the Intertropical Convergence Zone (ITCZ) as recorded by Lake Towuti δ13C$_{leaf\ wax}$ reported in this study (*11*). (**H**) Onset of burning in tropical Queensland, Australia (*15*). (**I**) Extinction of megafauna in Australia (and continental-wide aridification) (*13, 14*) and faunal turnover in southern Africa (*42*). SH, Southern Hemisphere. (**J**) Local glacial maxima in the southwest Pacific (*7, 10*) and the central Andes (*7, 10*). (**K**) Migration of mid-latitude westerly airflow equatorward from Auckland Islands (*12*) and possible extinction of subantarctic plant species (fig. S6). (**L**) West Antarctic (WAIS) δ18O (*41*). NGRIP and WAIS δ18O values reported on the GICC05 (+265 years) time scale (*41*). AIM, Antarctic isotopic maximum events. The Laschamps is shown in three phases: the transition phases (dark gray) on either side of the reversed polarity (light gray). The Mono Lake Excursion (34.6 ka) is also shown (light gray column) (*1*). Asterisks denote evidence of geomagnetic alteration associated with the Laschamps, demonstrating synchronous change across many parts of the globe.
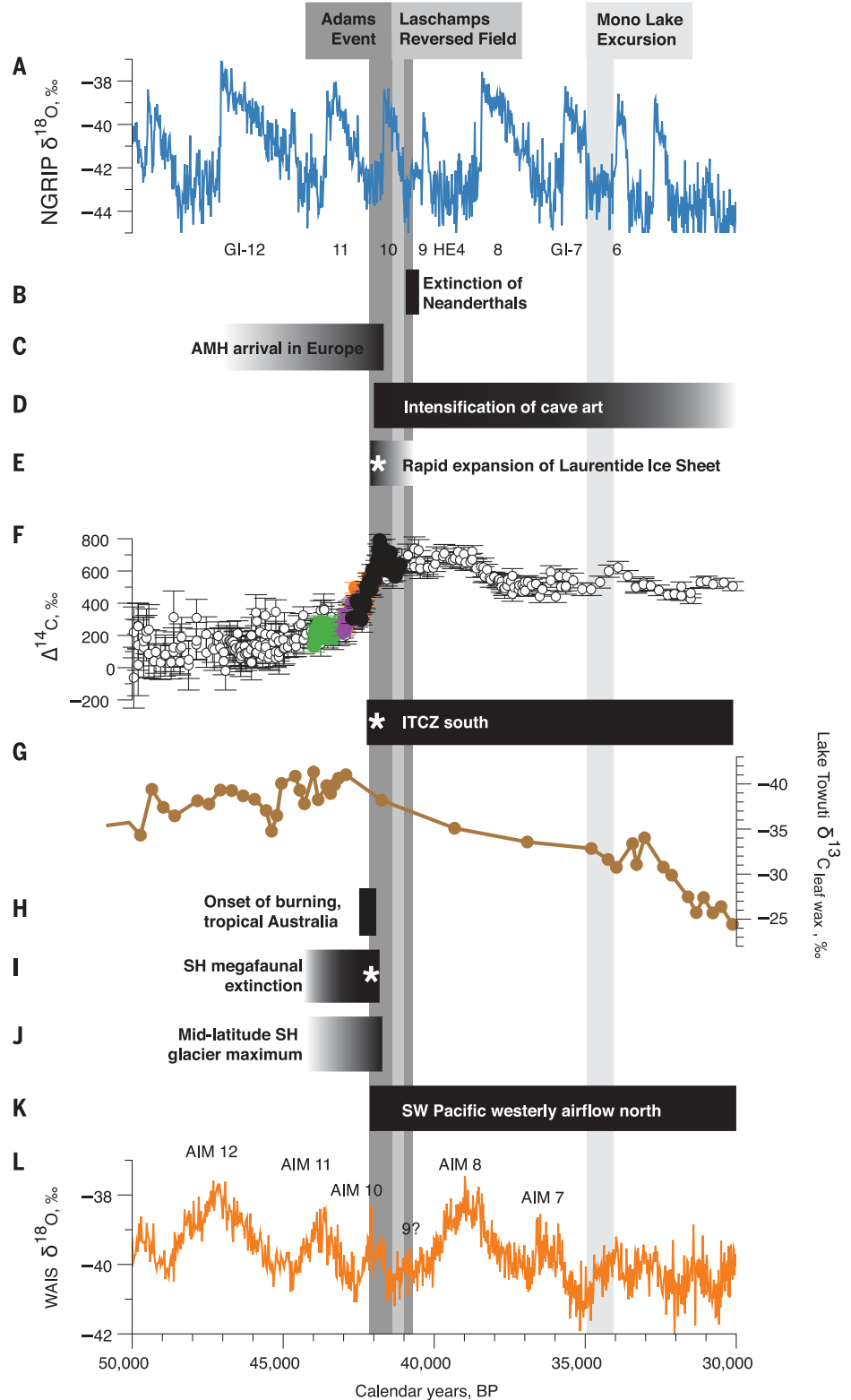
Laschamps from these confounding factors, we used the kauri-Hulu radiocarbon calibration curve to examine a transect of stratigraphically constrained sites in the Pacific (i.e., outside the Atlantic Ocean basin) from the subantarctic to the tropics (Fig. 4).

We used high-resolution radiocarbon dating to investigate Laschamps-aged sedimentary sequences at sites that record the behavior of both the Intertropical Convergence Zone (ITCZ) (Lake Towuti, Sulawesi) and mid-latitude Southern Hemisphere westerlies

(subantarctic Auckland Islands). On the subantarctic Auckland Islands (50°S) (see supplementary materials), which currently sit under Southern Hemisphere mid-latitude westerly airflow (*12*), a lignite sedimentary horizon at Pillar Rock records a warm period
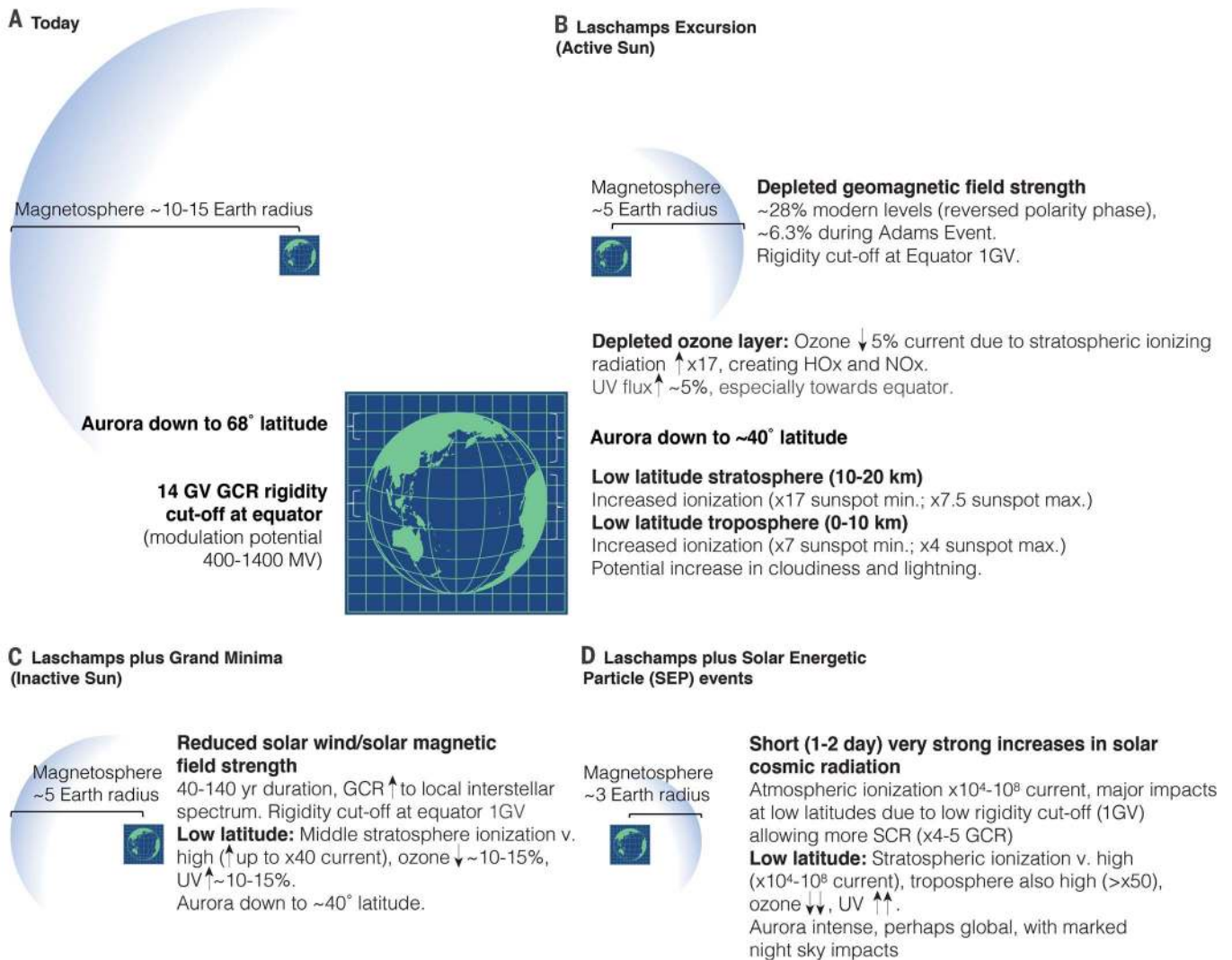
Fig. 5. Summarized potential impacts of different states of Earth's magnetic field and solar events. (**A** to **D**) Size of the magnetosphere, auroral extent, atmospheric ionization and associated chemistry and climate impacts for (A) today, (B) the Laschamps, (C) GSM during the Laschamps, and (D) major SEP events during the Laschamps (see supplementary materials). Upward arrows represent increase, and downward arrows represent decrease. max., maximum; min., minimum; SCR, solar cosmic radiation; GV, gigavolt; MV, megavolt.

from 54 to 42 ka within the last glaciation. Pollen records of *Dracophyllum* scrub grassland on this exposed cliff top and long-distance transport of lowland podocarp forest pollen from the New Zealand mainland indicate weaker westerly winds than now and mean annual temperatures within 1° to 1.5°C of those today (supplementary materials), interpreted to represent a period when the core of the Southern Hemisphere westerlies lay relatively poleward, delivering mid-latitude air masses over this sector of the Southern Ocean (*12*). A series of 12 contiguous ^{14}C ages reveals the upper stratigraphic boundary, marking a return to periglacial conditions that occurred at 42.23 ± 0.2 ka, coincident with the weakening of the magnetic field during

the transition phase into the Laschamps (Fig. 1). The periglacial conditions lasted until the Holocene (*12*), suggesting pervasive and widespread cold conditions (associated with a strengthening or northward shift in the core westerly airflow) across this sector of the Southern Ocean.

In the equatorial west Pacific, Lake Towuti currently experiences a wet season from December to May as the ITCZ migrates southward (*11*). During the last glacial period, Lake Towuti preserves a marked and sustained shift in $\delta^{13}C_{leaf\ wax}$ to more positive values (interpreted as representing more arid conditions), which persisted until the Pleistocene-Holocene boundary (Fig. 4 and supplementary materials) (*11*). A comprehensive series of 13

new radiocarbon dates and sediment magnetic intensity minima suggest that the ITCZ shift occurred at 42.35 ± 0.2 ka, again during the geomagnetic transition phase into the Laschamps (fig. S11), precisely aligning to the westerly airflow shift recorded at Pillar Rock. The high level of precision on the ages obtained for the major climatic boundaries recorded in Lake Towuti and the Auckland Islands is only possible because of the contiguous series of radiocarbon dates from each sequence, which permit accurate alignment against the steep rise in atmospheric radiocarbon values across this period (Fig. 1).

The above changes are consistent with a wealth of observations that indicate major environmental changes around the Pacific

Basin at the time of the geomagnetic transition into the Laschamps. For instance, a northward movement of the Southern Hemisphere westerlies has been proposed to explain the local peak glacial advance in the arid southern-central Andes, sometime before 39 ka (Fig. 4) (7) and tentatively related to fluxes in cosmic radiation and the Laschamps (8). Maximum glacial advances are also observed in New Zealand ~42 ka (10), consistent with the climate modeling of enhanced southwesterly airflow over the mid-latitudes (Fig. 3) (8). These broad-scale atmospheric circulation changes appear to have had far-reaching consequences. Within Australia, the peak megafaunal extinction phase is dated at ~42.1 ka, both in the mainland and Tasmania (Fig. 4) (14–16), and has generally been attributed to human action, although well after their initial arrival at least 50 ka (14, 16, 32). Instead, the megafaunal extinctions appear to be contemporaneous with a pronounced climatic phase shift to arid conditions that resulted in the loss of the large interior lakes and widespread change in vegetation patterns (13, 15). At Lynch's Crater in northeast Australia, the shift in vegetation structure, accompanied by increased burning (15), has been recalibrated here at 41.91 ± 0.4 ka, overlapping with the climatic boundaries observed at Lake Towuti and the Auckland Islands. Likewise, sediments at the Lake Mungo site associate the timing of the loss of Australia's interior lakes and megafaunal extinction phase with a reported geomagnetic excursion ~42 ka (locally called the "Lake Mungo Excursion") (supplementary materials) (13). Similar signals of marked floral and faunal change also appear to exist on New Caledonia and as far afield as South Africa (see supplementary materials). Together, these records suggest that both a mid-latitude climatic shift and major extinction phases overlap with the geomagnetic transition leading into the Laschamps, implying an association between these events.

Our model simulations potentially provide important insights into the global nature of the changes observed around the time of the Laschamps. Although the immediate impacts associated with the geomagnetic transition were likely on the order of the duration (800 years), many of the above synchronous changes persisted for millennia. This implies that a threshold may have been passed in one or more Earth system components, effectively tipping into a different persistent state (Fig. 4). One possibility is that with Earth's orbital configuration moving toward a full glacial state and limited global ocean ventilation (see supplementary materials), the climate system may have been sensitive to a relatively short but extreme forcing around the time of the Laschamps. For instance, terrestrial and marine sedimentary records have revealed that the LIS ex-

panded rapidly from a local minimum at 42 ka (18, 19) in association with a magnetic reversal (17, 19), with geological constraints and numerical models indicating that some parts of the ice sheet may have expanded >1000 km by ~39 to 37 ka (18). Although our model simulations do not suggest any major change in airflow over the equatorial and southern Pacific, we do find a substantially weakened polar vortex, most notably during the boreal winter (Fig. 3 and supplementary materials). The greatly reduced surface temperatures akin to a negative phase of the AO and NAO could potentially have created a positive feedback for ice sheet growth, reducing global sea levels. Recent work has suggested that a greatly expanded LIS would have reorganized atmospheric circulation across the wider Pacific Ocean (11). Such a hemisphere-wide response to abrupt forcing is consistent with the synchronous movement of the mid-latitude Southern Hemisphere westerlies determined from Pillar Rock and implied from glacial behavior in New Zealand, Australia, and the central Andes.

The Adams Transitional Geomagnetic Event and wider implications

Overall, the signals discussed above suggest that contemporaneous climatic and environmental impacts occurred across the mid- to lower latitudes ~42 ka, coincident with Earth's weakened geomagnetic field immediately preceding the reversed state of the Laschamps (Fig. 4). We describe this as the "Adams Transitional Geomagnetic Event" (hereafter "Adams Event"), named after the science writer Douglas Adams because of the timing (the number "42") and the associated range of extinctions (33). Previous studies may have failed to identify such a relationship between the Laschamps and climatic impacts because of the lack of temporal resolution and by focusing on the period of actual reversed geomagnetic field (41.5 to 41.1 ka) (5, 6) rather than the preceding extended phase of much weaker geomagnetic field (42.4 to 41.5 ka).

The lowered geomagnetic field intensity during the Adams Event, together with major changes in the intensity of cosmic radiation, is estimated to have increased levels of atmospheric ionization and ultraviolet (UV) radiation, especially in equatorial and low latitudes (<40°), because of a 10-fold decrease in the cosmic ray cut-off rigidity (Fig. 5 and supplementary materials). During GSM, the ionization in the middle stratosphere and surface UV radiation levels are estimated to have been further heightened (up to 25 to 40% and 10 to 15% above current levels, respectively), after taking into account changes in the solar spectrum. Furthermore, these values are likely to be much greater during the short-lived solar energetic particle (SEP)

events (Fig. 5 and supplementary materials). Although the relationship between increased atmospheric ionization and stratospheric and tropospheric cloudiness through cloud-seeding–type impacts remains uncertain, such impacts would be focused toward the lower latitudes (9), where the potential for lightning strikes could explain the increased records of charcoal observed around the Laschamps in Australia (15) and lack of relationship with archaeological signs of human activity (see supplementary materials).

The implications of this study are considerable. For instance, the Adams Event is very close in timing to the globally widespread appearance and increase in figurative cave art, red ochre handprints, and changing use of caves ~40 to 42 ka, e.g., in Europe and Island Southeast Asia (fig. S34 and supplementary materials) (34–36). This sudden behavioral shift in very different parts of the world is consistent with an increasing or changed use of caves during the Adams Event, potentially as shelter from the increase of ultraviolet B, potentially to harmful levels, during GSM or SEPs, which might also explain an increased use of red ochre sunscreen (4). Rather than the actual advent of figurative art, early cave art would therefore appear to represent the preservation of preexisting behaviors on a new medium (supplementary materials) (36). Other important archaeological boundaries during the wider Laschamps include the extinction of the Neanderthals (recalibrated here at 40.9 to 40.5 ka), along with the disappearance of some of the first European AMH cultures and the subsequent widespread appearance of the Aurignacian technocomplex (Fig. 4 and supplementary materials) (4, 31, 37).

The Adams Event appears to represent a major climatic, environmental, and archaeological boundary that has previously gone largely unrecognized. Furthermore, another well-known geomagnetic excursion in the recent past, Mono Lake (34 ka) (1), also appears to be marked by a distinct peak in the $\Delta^{14}C$ levels in the Hulu Cave stalagmite (Fig. 3) and aligns closely with a further latitudinal shift in the ITCZ as recorded in Lake Towuti, as well as a cluster of megafaunal extinctions in Eurasia (38) (supplementary materials). Importantly, geomagnetic transition phases can last substantially longer than during the Laschamps; for instance, the most recent full geomagnetic reversal, the Brunhes-Matuyama (at ~790 ka) (39) has a transition phase of ~20 ka, some 25 times longer than the Adams Event, with potentially far-reaching global climatic and evolutionary effects. The discovery that geomagnetic excursions can alter latitudinal temperature gradients through drastic increases in cosmic radiation and decreased ozone concentrations provides a new model for sudden paleoclimate

shifts. Overall, these findings raise important questions about the evolutionary impacts of geomagnetic reversals and excursions throughout the deeper geological record (*4*).

REFERENCES AND NOTES

1. C. Laj, H. Guillou, C. Kissel, *Earth Planet. Sci. Lett.* **387**, 184–197 (2014).
2. M. Brown, M. Korte, R. Holme, I. Wardinski, S. Gunnarson, *Proc. Natl. Acad. Sci. U.S.A.* **115**, 5111–5116 (2018).
3. E. J. Oughton, A. Skelton, R. B. Horne, A. W. P. Thomson, C. T. Gaunt, *Space Weather* **15**, 65–83 (2017).
4. J. E. T. Channell, L. Vigliotti, *Rev. Geophys.* **57**, 709–738 (2019).
5. J. Liu, N. R. Nowaczyk, S. Panovska, M. Korte, H. W. Arz, *J. Geophys. Res.* **125**, e2019JB019225 (2020).
6. G. Wagner, D. M. Livingstone, J. Masarik, R. Muscheler, J. Beer, *J. Geophys. Res.* **106**, 3381–3387 (2001).
7. R. Zech, J. Zech, C. Kull, P. W. Kubik, H. Veit, *Clim. Past* **7**, 41–46 (2011).
8. I. Suter, R. Zech, J. Anet, T. Peter, *Clim. Past* **10**, 1183–1194 (2014).
9. J. Kirkby *et al.*, *Nature* **533**, 521–526 (2016).
10. P. D. Strand *et al.*, *Quat. Sci. Rev.* **220**, 165–177 (2019).
11. J. M. Russell *et al.*, *Proc. Natl. Acad. Sci. U.S.A.* **111**, 5100–5105 (2014).
12. E. Rainsley *et al.*, *Clim. Past* **15**, 423–448 (2019).
13. J. M. Bowler *et al.*, *Nature* **421**, 837–840 (2003).
14. F. Saltré *et al.*, *Nat. Commun.* **7**, 10511 (2016).
15. S. Rule *et al.*, *Science* **335**, 1483–1486 (2012).
16. C. S. M. Turney *et al.*, *Proc. Natl. Acad. Sci. U.S.A.* **105**, 12150–12153 (2008).
17. H. W. Hill, B. P. Flower, T. M. Quinn, D. J. Hollander, T. P. Guilderson, *Paleoceanography* **21**, PA1006 (2006).
18. A. S. Dalton *et al.*, *Geology* **47**, 111–114 (2019).
19. A. S. Dalton, S. A. Finkelstein, P. J. Barnett, S. L. Forman, *Quat. Sci. Rev.* **146**, 288–299 (2016).
20. G. M. Raisbeck *et al.*, *Clim. Past* **13**, 217–229 (2017).
21. F. Adolphi *et al.*, *Clim. Past* **14**, 1755–1781 (2018).
22. H. Cheng *et al.*, *Science* **362**, 1293–1297 (2018).
23. R. A. Staff *et al.*, *Earth Planet. Sci. Lett.* **520**, 1–9 (2019).
24. A. M. Lorrey *et al.*, *Quat. Sci. Rev.* **183**, 124–139 (2018).
25. C. S. M. Turney *et al.*, *Sci. Rep.* **8**, 3293 (2018).
26. K. Kodera, Y. Kuroda, *J. Geophys. Res.* **107**, ACL 5-1–ACL 5-12 (2002).
27. J. Kidston *et al.*, *Nat. Geosci.* **8**, 433–440 (2015).
28. V. Masson-Delmotte *et al.*, *Science* **309**, 118–121 (2005).
29. S. O. Rasmussen *et al.*, *Quat. Sci. Rev.* **106**, 14–28 (2014).
30. G. Deplazes *et al.*, *Nat. Geosci.* **6**, 213–217 (2013).
31. M. Staubwasser *et al.*, *Proc. Natl. Acad. Sci. U.S.A.* **115**, 9116–9121 (2018).
32. J. F. O'Connell *et al.*, *Proc. Natl. Acad. Sci. U.S.A.* **115**, 8482–8490 (2018).
33. D. Adams, M. Carwardine, *Last Chance to See* (Arrow Books, 2009).
34. A. W. Pike *et al.*, *Science* **336**, 1409–1413 (2012).
35. S. O'Connor, R. Ono, C. Clarkson, *Science* **334**, 1117–1121 (2011).
36. M. Aubert *et al.*, *Nature* **564**, 254–257 (2018).
37. J.-J. Hublin *et al.*, *Nature* **581**, 299–302 (2020).
38. A. Cooper *et al.*, *Science* **349**, 602–606 (2015).
39. B. S. Singer, B. R. Jicha, N. Mochizuki, R. S. Coe, *Sci. Adv.* **5**, eaaw4621 (2019).
40. K. Hughen *et al.*, *Science* **303**, 202–207 (2004).
41. WAIS Divide Project Members, *Nature* **520**, 661–665 (2015).
42. J. T. Faith, *J. Hum. Evol.* **65**, 715–730 (2013).

SUPPLEMENTARY MATERIALS

science.sciencemag.org/content/371/6531/811/suppl/DC1
Materials and Methods
Figs. S1 to S34
Tables S1 to S8
References (*43–175*)

24 March 2020; accepted 14 December 2020
10.1126/science.abb8677

Science

A global environmental crisis 42,000 years ago

Alan Cooper, Chris S. M. Turney, Jonathan Palmer, Alan Hogg, Matt McGlone, Janet Wilmshurst, Andrew M. Lorrey, Timothy J. Heaton, James M. Russell, Ken McCracken, Julien G. Anet, Eugene Rozanov, Marina Friedel, Ivo Suter, Thomas Peter, Raimund Muscheler, Florian Adolphi, Anthony Dosseto, J. Tyler Faith, Pavla Fenwick, Christopher J. Fogwill, Konrad Hughen, Mathew Lipson, Jiabo Liu, Norbert Nowaczyk, Eleanor Rainsley, Christopher Bronk Ramsey, Paolo Sebastianelli, Yassine Souilmi, Janelle Stevenson, Zoë Thomas, Raymond Tobler and Roland Zech

Reversing the field

Do terrestrial geomagnetic field reversals have an effect on Earth's climate? Cooper *et al.* created a precisely dated radiocarbon record around the time of the Laschamps geomagnetic reversal about 41,000 years ago from the rings of New Zealand swamp kauri trees. This record reveals a substantial increase in the carbon-14 content of the atmosphere culminating during the period of weakening magnetic field strength preceding the polarity switch. The authors modeled the consequences of this event and concluded that the geomagnetic field minimum caused substantial changes in atmospheric ozone concentration that drove synchronous global climate and environmental shifts.
Science, this issue p. 811

ARTICLE TOOLS	http://science.sciencemag.org/content/371/6531/811
SUPPLEMENTARY MATERIALS	http://science.sciencemag.org/content/suppl/2021/02/17/371.6531.811.DC1
RELATED CONTENT	http://science.sciencemag.org/content/sci/371/6531/766.full
REFERENCES	This article cites 163 articles, 25 of which you can access for free http://science.sciencemag.org/content/371/6531/811#BIBL
PERMISSIONS	http://www.sciencemag.org/help/reprints-and-permissions

Use of this article is subject to the Terms of Service